Journal of Applied Polymer Science

Largely Improved Crystallization Behavior and Thermal Stability of Poly(L-Lactide) Via the Synergistic Effects of Graphene Oxide and Carbon Nanotubes

Hai-Ming Chen,[1] Li-Na Shao,[1] Ying Shen,[1] Jing-Hui Yang,[1] Ting Huang,[1] Nan Zhang,[1] Yong Wang,[1] Chao-liang Zhang[2]

[1]Key Laboratory of Advanced Technologies of Materials (Ministry of Education), School of Materials Science and Engineering, Southwest Jiaotong University, Chengdu 610031, China

[2]State Key Laboratory of Oral Diseases, Sichuan University, Chengdu 610041, China

Correspondence to: Y. Wang (E-mail: yongwang1976@163.com)

ABSTRACT: Graphene oxide (GO) and carbon nanotubes (CNTs) and their compound were introduced into semicrystalline poly (L-lactide) (PLLA) to prepare the corresponding binary and/or ternary nanocomposites, respectively. The dispersion states of nanofillers in different nanocomposites were investigated using UV-Vis spectroscopy, scanning electron microscopy (SEM) and rheological measurement. The results showed that when GO and CNTs were simultaneously present in the PLLA matrix, good dispersion states of both GO and CNTs could be achieved and the ternary nanocomposites exhibited percolated network structure. The effects of different nanofillers on the crystallization behavior of PLLA matrix were comparatively investigated under the different crystallization conditions including melt crystallization process (nonisothermal and isothermal crystallization from the melt) and cold crystallization (crystallization occurring from an amorphous state during the annealing process). The results showed that GO and CNTs exhibited apparent synergistic effects in improving crystallization ability and enhancing crystallinity of PLLA matrix. Study on the thermal stability of nanocomposites showed that the presence of nanofillers greatly improved the thermal stability of PLLA matrix. © 2013 Wiley Periodicals, Inc. J. Appl. Polym. Sci. **2014**, *131*, 40143.

KEYWORDS: polyesters; crystallization; thermal properties

Received 15 April 2013; accepted 30 October 2013

DOI: 10.1002/app.40143

INTRODUCTION

Polymer-based nanocomposites have attracted much attention of researchers in both the academic and industry fields due to their novel microstructures and excellent comprehensive properties. The key issues to achieve the materials with expected performance are believed to be those which nanofiller has good dispersion in the polymer matrix and there is an appropriate interfacial interaction between polymer and nanofiller. Factually, the good interaction also facilitates to the good dispersion of nanofiller.

Recent researches have shown that with the combination effects of different nanofillers with different dimensions in one polymer matrix, the novel nanocomposite usually exhibits special microstructures of nanofillers and dramatically improved properties. Among these nanofillers, the simultaneous addition of one-dimensional carbon nanotubes (CNTs) and two-dimensional montmorillonite (OMMT) or clay is specially focused and the corresponding nanocomposites have been researched for a long time.[1–10] It has been proved that there is a certain interaction between CNTs and OMMT, which facilitates the formation of network structure of nanofillers at smaller concentration in the polymer matrix on the one hand.[11] On the other hand, some researches prove that addition of OMMT also facilitates the good dispersion of CNTs.[12] Due to the relatively higher aspect ratio and specific surface area of CNTs compared with OMMT, achieving the good dispersion of CNTs is expected to be favorable for the improvement of crystallization and mechanical properties of semicrystalline polymers.

As one of the allotropes of carbon material, graphene oxide (GO) has similar chemical structure to CNTs on the one hand. Therefore, it is believed to be that the interaction between GO and CNTs is most likely stronger than that between CNTs and OMMT. On the other hand, there are much functional groups on the surface of GO, which facilitates the dispersion of GO in the polar polymer matrix. This also indicates that the combination effects of GO and CNTs in one polymer matrix deserves consideration. For example, Yang et al. proved that GO and CNTs exhibit

synergistic effects in improving the mechanical and thermal properties of epoxy nanocomposites.[13] Specifically, it has been proved that GO has great potential in improving the good dispersion of CNTs in different conditions.[14–16] Zhang et al. developed a facile method to prepare the poly(vinyl alcohol) (PVA) nanocomposite with reduced GO and functionalized CNTs simultaneously and found that the nanocomposite exhibited homogeneous dispersion of nanofiller. As a consequence, significantly improved tensile strength and Young's modulus were achieved.[17]

Poly(L-lactide) (PLLA), which is one of the biodegradable and biocompatible thermoplastic polymers, can be prepared from completely natural sources such as corn, wheat and/or rice, and therefore it reduces the degree of dependence on petroleum sources. Hence, PLLA has generated numerous scientific activities. However, the application of PLLA is greatly limited by its poor crystallization behavior and thermal properties. CNTs have been proved to be an efficient nucleating agent for the crystallization of PLLA whether in the melt crystallization process or in the cold crystallization process.[18–21] The enhancement of crystallization behavior of PLLA is dependent upon many factors, such as the modification of CNTs, the aspect ration of CNTs and the content of CNTs.[22–27] It is also proved that CNTs also facilitate the improvement of the thermal stability of PLLA.[28,29] GO also exhibits nucleation effect in accelerating the crystallization of PLLA.[30,31] However, the ability of CNTs to induce crystallization is stronger than that of GO.[32] Simultaneous addition of different nanofillers with different dimensions into PLLA also attracts the interests of researchers. For example, Kim et al. introduced CNTs and clay into PLLA and found that the ternary nanocomposites showed superior tensile properties.[33] Hapuarachchi and Peijs found that PLLA ternary nanocomposites with clay and CNTs showed a great reduction in peak heat release when tested in the cone calorimeter.[34] Santangelo et al. synthesized a kind of hybrid nanofiller with direct growth of CNTs over clay and introduced the hybrid nanofiller into PLLA. The results showed that PLLA nanocomposites were endowed with increased sorption and outstandingly enhanced conductivity.[35] However, the combination effects of different nanofillers on the crystallization behavior of PLLA are less reported.

Due to their large aspect ratio and relatively soft chain structure, CNTs have a tendency to change their conformation and aggregate together, forming the agglomerate. This decreases the nucleation ability of CNTs in accelerating the crystallization of PLLA. Illuminating by the positive role of GO in assisting the dispersion of CNTs in other polymer matrix, in this work, we attempted to introduce GO and CNTs into PLLA simultaneously to prepare the ternary nanocomposite. Our attention was focused on the change of thermal properties and the crystallization behavior of PLLA matrix. Interestingly, it was found that there were synergistic effects of GO and CNTs in improving the crystallization behavior and thermal stability of PLLA matrix.

EXPERIMENTAL

Materials

PLLA (3051D, D-isomer content = 3.3%, with molecular weight (M_w) of 2.53 × 10^5 g/mol, melt flow rate (MFR) of 14 g/10min (210°C/2.16 kg) and density of 1.24 g/cm^3) was purchased from NatureWorks®. Graphite was obtained from Qingdao Heilong Graphite Co., Ltd. Pristine CNTs were obtained from Chengdu Institute of Organic Chemistry, Chinese Academy of Science (Chengdu, China). The outer and inner diameters of CNTs are 20 to 30 nm and 5 to 10 nm, respectively. The length of a single CNT is about 10 to 50 μm. MWCNTs were washed and purified with concentrated hydrochloride acid, and the purity is above 95%.

Sample Preparation

GO was prepared in our laboratory according to Hummer's method[36] and the corresponding data of GO can be seen in our previous work.[37] Functionalized CNTs were first prepared through the chemical modification method which was developed in our previous work.[38] After the chemical modification, some polar groups including carboxyl and hydroxyl groups were introduced to the surface of GO and CNTs, which was proved to be favorable for the good dispersion of both GO and CNTs in the nanocomposites. The weight fractions of functional groups on the surface of GO and CNTs were about 34.59% and 1.73%, respectively.

Samples were prepared through the solution-mixing method. First, GO, CNTs and PLLA were dissolved in the DMF to prepare the solution of GO/DMF, CNTs/DMF and PLLA/DMF, respectively; then the solution of GO/DMF and PLLA/DMF was compounded together with stirring at 70°C for 2 h; and then the mixture was dried at 100°C until the solvent was removed completely. Finally, the nanocomposite of PLLA/GO was prepared. Through the completely same procedures, nanocomposites of PLLA/CNTs and PLLA/GO/CNTs were also prepared. For making a comparison, it should be stressed that PLLA sample was also prepared through the completely same procedures. In this work, the weight fraction of nanofiller in the binary nanocomposites is 2.0 wt %. For the ternary nanocomposite, the weight fraction of each nanofiller is 1.0 wt %. The sample notation and the compositions of the nanocomposites can be seen in Table I. To prepare the sample for the measurement, the nanocomposites were first heated to melt completely. Subsequently, some nanocomposites were immersed directly into ice-water to obtain the amorphous samples and others were directly transferred into a hot-stage with the temperature of 105°C and maintained at this temperature for 30 min. After that, the isothermal-crystallized samples were taken out and cooled to room temperature in an atmosphere condition. In addition, some quenched amorphous samples were further annealed in an oven at 120°C for 30 min, and then the annealed samples were taken out and cooled to room temperature.

UV-Vis Spectroscopy

The dispersion state of nanofiller in the DMF solvent was first investigated using UV-Vis spectroscopy (UV-1800PC

Table I. Sample Notation and the Compositions of the Samples

Samples	PLLA (wt %)	GO (wt %)	CNTs (wt %)
PLLA	100	0	0
PLLA/GO	98	2	0
PLLA/CNTs	98	0	2
PLLA/GO/CNTs	98	1	1

SPECTROPHOTOMETER) in the wavelength range of 350 to 600 nm. The concentration of nanofiller in the solution was maintained as 0.008 mg/mL. For GO/CNTs system, the weight ratio between GO and CNTs is 1 : 1, namely, the concentrations of GO and CNTs are 0.004 mg/mL, respectively.

Scanning Electron Microscopy (SEM)

The distribution of both GO and CNTs in the PLLA matrix was investigated using a scanning electron microscope (SEM, Fei Inspect FEI, The Netherlands) with an accelerating voltage of 5.0 kV. The sample was first cryogenically fractured in liquid nitrogen, and then the fractured surface was coated with a thin layer of gold before SEM characterization.

Rheological Measurement

The rheological measurement was carried out on a stress controlled rheometer (AR2000ex). The sample disk was firstly prepared with a thickness of 2 mm and a diameter of 20 mm through a compression molding way at the melt temperature of 190°C and a pressure of 5 MPa. During the rheological measurement process, the frequency sweep from 0.05 to 300 rad/s was performed at 180°C under dry nitrogen atmosphere. For all the measurements, the samples were tested within the linear viscoelastic strain range.

Differential Scanning Calorimetry (DSC)

Differential scanning calorimetry (DSC, Netzsch STA 449C Jupiter, Germany) was used to investigate the melting and crystallization behaviors of PLLA nanocomposites. For the unannealed sample, it was first heated from 0 to 200°C at a heating rate of 10°C/min and maintained at 200°C for 3 min to erase any thermal history, then the sample was cooled to 0°C at a cooling rate of 2°C/min, and then the sample was heated again to 200°C at the heating rate of 10°C/min. The second heating curve was analyzed. For the isothermal-crystallized and annealed samples, they were directly heated from 0 to 200°C at the heating rate of 10°C/min. All the DSC measurements were carried out in nitrogen atmosphere and the weight of each sample was about 8 mg. The value of degree of crystallinity (X_{c-DSC}) of PLLA was calculated according to the following equation:

$$X_{c-DSC}=\frac{\Delta H_m-\Delta H_{cc}}{\Delta H_m^0\times\phi}\times 100\% \quad (1)$$

where ΔH_m is the DSC measured value of fusion enthalpy, ΔH_{cc} is the cold crystallization enthalpy obtained during the DSC heating process, ΔH_m^0 is the fusion enthalpy of the completely crystalline PLLA, and ϕ is the weight fraction of PLLA in the sample. Here, the value of ΔH_m^0 of PLLA was selected as 93 J/g [39].

Wide Angle X-Ray Diffraction (WAXD)

The crystalline structure of PLLA in different samples was investigated using a wide angle X-ray diffraction (WAXD, DX-1000 with Ni-filtered Cu Kα radiation, China). The continuous scanning angle range used in this study was from 5° to 30° at 40 kV and 25 mA. The X_{c-WAXD} was calculated according to the following relation:

$$X_{c-WAXD}=\frac{\sum A_{crystalline}}{\sum A_{crystalline}+\sum A_{amorphous}}\times 100\% \quad (2)$$

where $A_{crystalline}$ and $A_{amorphous}$ are the fitted areas of the diffraction peaks of crystalline and amorphous, respectively.

Thermogravimetric Analysis (TGA)

In order to study the thermal stability of the sample, the thermogravimetric analysis (TGA) measurement was carried out using the TA instrument (TGA, Q500) in nitrogen atmosphere. Sample was heated from 30 to 450°C and different heating rates, i.e. 10, 20, 30, and 40°C/min, were selected.

RESULTS AND DISCUSSION

Dispersion of Nanofiller in PLLA Matrix

The dispersion of nanofiller was first evaluated using UV-Vis spectra measurement and the results are shown in Figure 1. The inserted images show the comparison of suspensions of nanofillers in the DMF. Generally, the absorption intensity is proportional to the concentration of nanofiller in the solution. In this work, although all the nanofiller/DMF solutions have the same concentration of nanofiller, single GO sheet has relatively larger mass and dimension compared with single CNT and most likely, the concentration of CNT in the unit volume is larger than that of GO on the one hand. On the other hand, the variation of absorption intensity is also related to the dispersion of nanofiller. The higher the absorption intensity, the better the dispersion of nanofiller is. As shown in Figure 1, GO exhibits the smaller absorption intensity compared with CNTs, indicating that the concentration of GO sheet in the unit volume and/or the dispersion of GO in the DMF solution is smaller than that of CNTs. Interestingly, it is observed that the absorption intensity of GO/CNTs/DMF solution is the strongest one, indicating that the concentration of nanofiller in the unit volume is the biggest one and/or the dispersion of GO/CNTs is the best one.

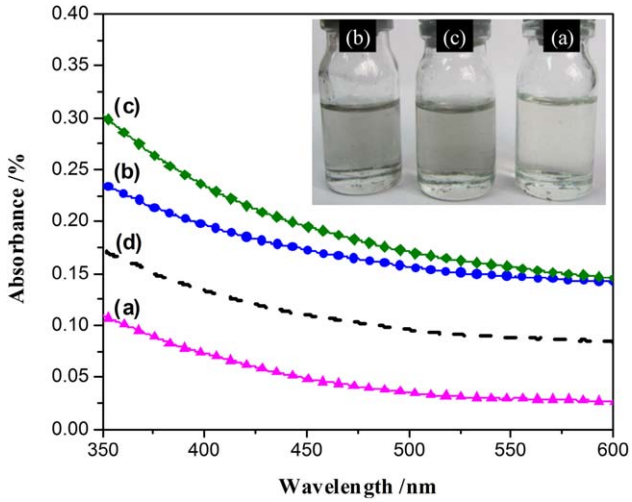

Figure 1. UV-Vis absorption spectra of (a) GO, (b) CNTs, and (c) GO/CNTs. (d) Shows the theoretical calculation of absorption intensity of GO/CNTs according to the linear superposition relation. The concentration of nanofiller in solution is 0.008 mg/mL. [Color figure can be viewed in the online issue, which is available at wileyonlinelibrary.com.]

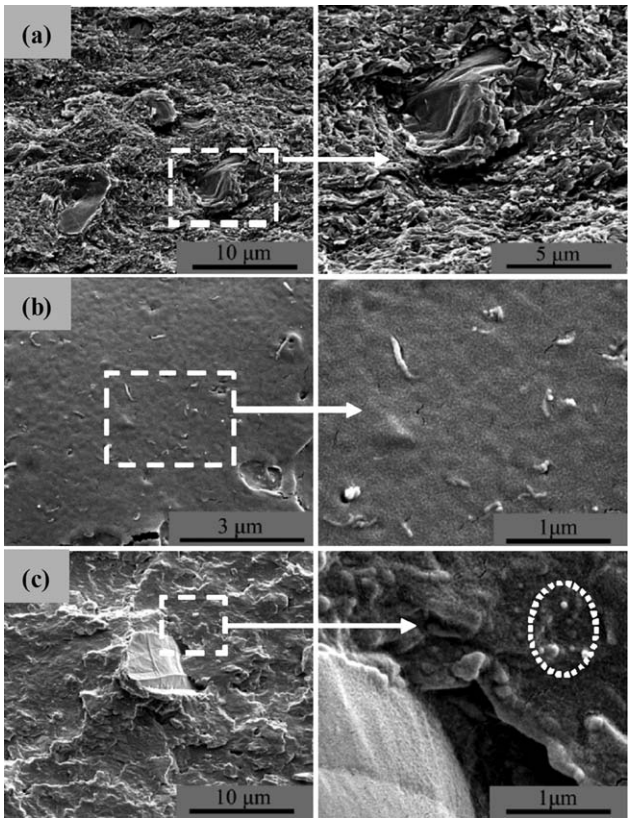

Figure 2. SEM images show the dispersion states of (a) GO, (b) CNTs, and (c) GO/CNTs in the PLLA matrix. The images in the right side were obtained at higher magnifications.

Since the concentrations of GO and CNTs in the GO/CNTs/DMF solution are 0.004 mg/mL, only a half of the concentration in the GO/DMF or CNTs/DMF solution, the theoretical calculation of absorption intensity of GO/CNTs/DMF solution can be calculated by linear superposition relation and the results are also shown in Figure 1 (dash line). It is clearly seen that the experimental data is much larger than those obtained from theoretical calculation. This indicates undoubtedly that when GO and CNTs are present simultaneously, the dispersion of GO/CNTs is enhanced. Zhang et al. has reported the similar results and they suggest that the GO sheets have a tendency to stabilizing CNTs with larger diameters.[16,17]

The dispersion of GO, CNTs, and GO/CNTs in the PLLA matrix were further investigated using SEM and the results are shown in Figure 2. It is clearly seen that both GO and CNTs exhibit good dispersion in the PLLA matrix. For PLLA/GO nanocomposites, although it is very difficult to differentiate the sheet number of GO agglomerate, it can be seen that GO sheets are well wetted by PLLA matrix and there is no apparent interface between GO and PLLA, indicating the good interfacial interaction between PLLA matrix and GO sheets. Even for PLLA/CNTs nanocomposite with 2.0 wt % CNTs, there is no serious aggregation of CNTs can be observed. For PLLA/GO/CNTs nanocomposite, the contents of both GO and CNTs in the unit area are reduced due to the decrease of concentration in the matrix. Similarly, no serious aggregation of nanofiller is observed. Specifically, one can see that CNTs have a tendency to disperse around GO sheet.

Generally, nanofillers with large aspect ratio lean to form the network structure in the polymer matrix, and such special microstructure can be deduced by rheological measurement. In this work, the rheological measurement was carried out and the results are shown in Figure 3. It can be seen that nanocomposites exhibit much higher storage modulus (G') compared with pure PLLA, indicating the increase of elastic properties of samples with the presence of nanofillers. However, the increase of G' is dependent upon the type of nanofiller. PLLA/GO sample exhibits much higher G' compared with PLLA/CNTs sample. Specifically, one can observe an apparent plateau in modulus curve of PLLA/GO sample at low frequency. Interestingly, it is observed that PLLA/GO/CNTs sample exhibits similar G' and loss modulus (G'') to PLLA/GO sample. The analogous Cole-Cole plots of G' versus G'' with frequency as a parameter are shown in Figure 3(c). It has been reported that the shift and the change in the slope of the Cole-Cole plots indicate the significant microstructure changes of the samples with addition of nanofillers.[40–42] PLLA/GO sample exhibits larger G' than G'', and the phenomenon becomes more apparent in the PLLA/GO/CNTs sample. Now, it is widely accepted that both the plateau at low frequency region of modulus curve and the deviation from a linear relationship between G' and G'' are indicative of the formation of a percolated network structure of nanofiller.[43–45] This means that the percolated network structure is formed in both PLLA/GO and PLLA/GO/CNTs samples. The variation of the microstructure can be further proved by the significant increase of complex viscosity (η^*) of the samples. Both PLLA/GO and PLLA/GO/CNTs samples exhibit much higher η^* compared with pure PLLA and PLLA/CNTs samples, further indicating the formation of percolated network structure which restricts the motion of PLLA chain segments. Importantly, all the rheological data prove that PLLA/GO/CNTs sample exhibits similar rheological properties to those of PLLA/GO sample. It should be stressed that the content of GO in the PLLA/GO/CNTs sample is only a half of that in PLLA/GO sample. Obviously, the simultaneous presence of GO and CNTs facilitates the formation of percolated network structure, contributing to the increase of modulus and viscosity. This is very similar to the synergistic effects of CNTs and OMMT in promoting the formation of percolated network structure.[11]

The dispersion states of nanofillers in different sample are further illustrated in Figure 4. Due to the large dimension of single GO sheet and the good dispersion of GO in the matrix, which provides the probability for GO sheets to contact each other, GO sheets form the so called network structure in the PLLA/GO sample. Although pristine CNTs also have the large aspect ratio, the surface modification process damages the long chain structure of CNTs. Furthermore, CNTs also exhibit good dispersion in the PLLA/CNTs sample. For PLLA/GO/CNTs sample, although the contents of both GO and CNTs are reduced and the probability for the formation of GO network structure is also reduced, some CNTs mainly dispersed between GO sheets as proved by SEM characterization, forming the hybrid network structure of GO/CNTs in the PLLA matrix. Specifically, with the

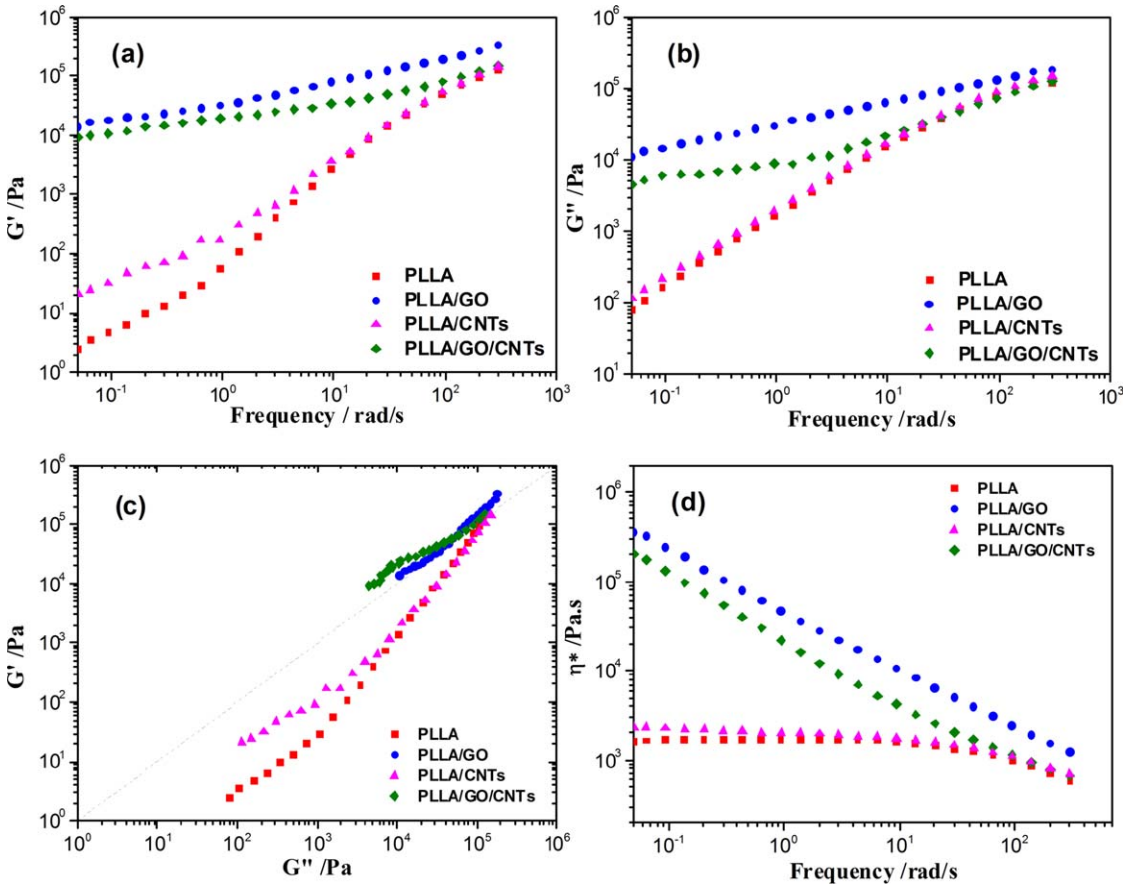

Figure 3. Rheological properties of different samples as indicated in the graphs. (a) Storage modulus, (b) loss modulus, (c) Cole-Cole plots of storage modulus versus loss modulus, and (d) complex viscosity. [Color figure can be viewed in the online issue, which is available at wileyonlinelibrary.com.]

presence of GO, the dispersion of CNTs becomes more homogeneous. Obviously, the hybrid network structure of GO/CNTs most likely results in the apparent changes of the thermal properties of PLLA matrix. This will be analyzed in detail in the next sections.

Crystallization Behavior of PLLA Matrix

PLLA is a typical polymorphic material with crystalline forms of α, β, and γ. When the crystallization occurs at temperature below 120°C, another new crystal form, i.e. αÇ-form, is also observed.[46–49] αÇ-form PLLA has the same conformation as in α-form but a loose packing manner compared to the α-form PLLA, and the two crystal modifications can be differentiated by means of infrared spectroscopy (IR) and WAXD.[50] For example, αÇ-form PLLA has relatively lower 2θ values of both (110)/(200) and (203) crystal planes compared with α-form PLLA. The crystallization of PLLA is relatively difficult and usually the amorphous PLLA articles are obtained through the common extrusion-injection molding processing due to the relatively large cooling rate which provides little time for the nucleation

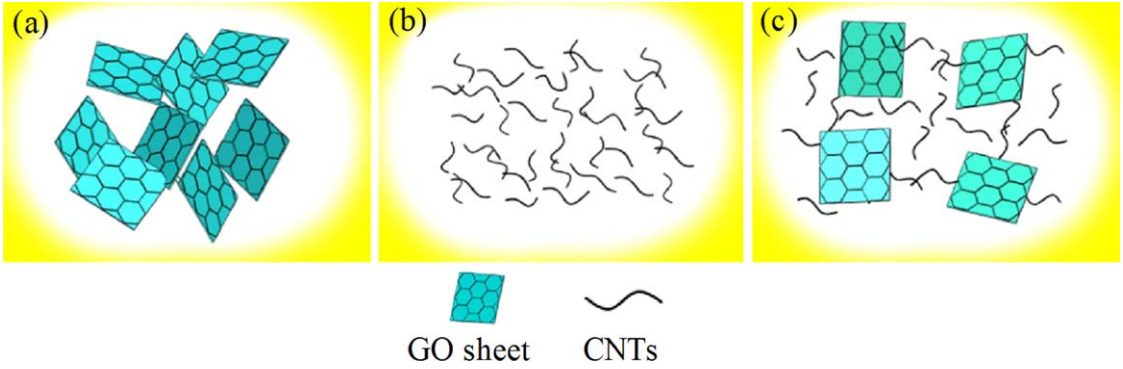

Figure 4. Schematic representations show the different dispersion states of (a) GO, (b) CNTs, and (c) GO/CNTs in the PLLA matrix. [Color figure can be viewed in the online issue, which is available at wileyonlinelibrary.com.]

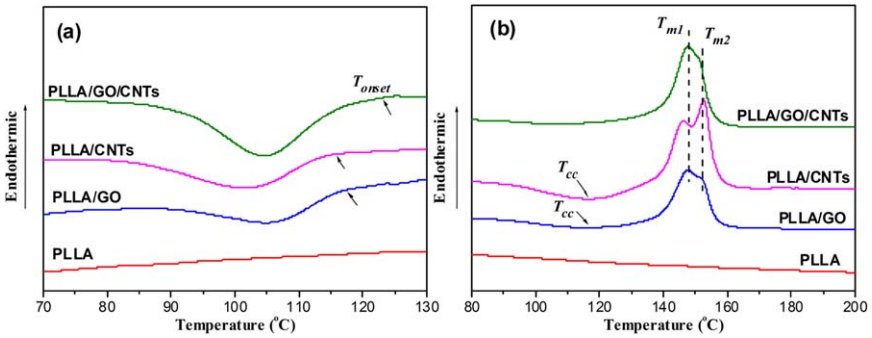

Figure 5. (a) DSC cooling curves of different samples obtained at cooling rate of 2°C/min and (b) subsequent heating curves obtained at a heating rate of 10°C/min. [Color figure can be viewed in the online issue, which is available at wileyonlinelibrary.com.]

and growth of PLLA crystallites.[51] In this work, to well understand the crystallization behavior of PLLA matrix in different nanocomposites, the crystallization behavior of samples were comparatively investigated under the different crystallization conditions including melt crystallization (nonisothermal and isothermal crystallization) and cold crystallization (crystallization from the amorphous state during the annealing process).

Figure 5 shows the crystallization and subsequent melting behaviors of different samples. The corresponding crystallization and melting parameters are shown in Table II. For making a comparison, the results of pure PLLA are also shown. From Figure 5(a) one can see that for pure PLLA, there is no any exothermic phenomenon attributing to the crystallization of PLLA. However, an apparent exothermic phenomenon is observed for all the PLLA nanocomposites, indicating the crystallization occurring during the cooling process. This clearly proves the heterogeneous nucleation effects of nanofillers for PLLA crystallization. However, the crystallization behavior of PLLA matrix is dependent upon the type of nanofiller. PLLA/GO sample exhibits the crystallization peak temperature (T_c) of 105.0°C, higher than the 101.8°C of PLLA/CNTs sample, indicating that GO sheets have more apparent nucleation effect for PLLA crystallization. This can be further proved by the enhanced crystallization start temperature (T_{onset}) and decreased peak width at half height ($W_{1/2h}$) of PLLA/GO sample (117.1 and 15.6°C, respectively) compared with PLLA/CNTs sample (115.9 and 17.5°C, respectively). Interestingly, it is observed that PLLA/GO/CNTs sample exhibits similar values of T_c and T_{onset} to those of PLLA/GO sample on the one hand; On the other hand, PLLA/GO/CNTs exhibits smaller $W_{1/2h}$ compared with other two nanocomposites, indicating the increased crystallization rate of the PLLA matrix in PLLA/GO/CNTs sample. The absolute value of enthalpy of crystallization (ΔH_c) of PLLA/GO/CNTs (25.1 J/g) is much larger than that of PLLA/GO (15.2 J/g) and PLLA/CNTs (17.0 J/g). This indicates that more PLLA crystallize during the cooling process.

The subsequent melting behaviors shown in Figure 5(b) further prove the changes of the crystalline structures in different samples. As expected, no endothermic peak is observed for pure PLLA. For the PLLA/GO sample, a weak exothermic peak (T_{cc}) at about 115.4°C, attributing to the cold crystallization of PLLA during the DSC heating process. This indicates that the crystallization of PLLA matrix during the melt crystallization process is not finished and some PLLA chain segments further crystallize during the DSC heating scan. Furthermore, an apparent endothermic peak is observed at 147.5°C (T_{m1}) with a shoulder at 151.3°C (T_{m2}). For the PLLA/CNTs sample, the exothermic peak at T_{cc} of 116.6°C is highly intensified, indicating that more PLLA crystallizes through the cold crystallization process. In other words, less PLLA crystallizes during the melt crystallization process as compared with the PLLA/GO sample. Similarly, double endothermic peaks are observed at 146.3°C and 152.6°C, and the latter one has stronger intensity. This can be attributed to the melting-recrystallization-melting process of PLLA crystallites during the DSC measurement. The PLLA/GO/CNTs sample also exhibits a weak exothermic peak but the value of T_{cc} (106.1°C) is largely reduced compared with the other two binary nanocomposites. The X_{c-DSC} was calculated with the deduction of the effect of cold crystallization on crystallinity. The data of X_{c-DSC} for PLLA/GO, PLLA/CNTs and PLLA/GO/CNTs are 15.5, 21.8, and 27.2%, respectively. It should be stressed that due to the melting-recrystallization-melting phenomenon occurred during the DSC heating scan, the X_{c-DSC} obtained by eq. (1) is the relative value rather than

Table II. The Crystallization and Melting Parameters of Samples Obtained During the DSC Measurements

Samples	T_{onset} (°C)	T_c (°C)	$W_{1/2h}$ (°C)	ΔH_c (J/g)	T_m (°C)	ΔH_{CC} (J/g)	T_m (°C)	ΔH_m (J/g)	X_{c-DSC} (%)
PLLA	–	–	–	–	–	–	–	–	0.0
PLLA/GO	117.1	105.0	15.6	−15.2	115.4	4.5	147.5/151.3	18.6	15.5
PLLA/CNTs	115.9	101.8	17.5	−17.0	116.6	9.4	146.3/152.6	29.3	21.8
PLLA/GO/CNTs	121.6	105.4	13.1	−25.1	106.1	2.0	147.8	26.8	27.2

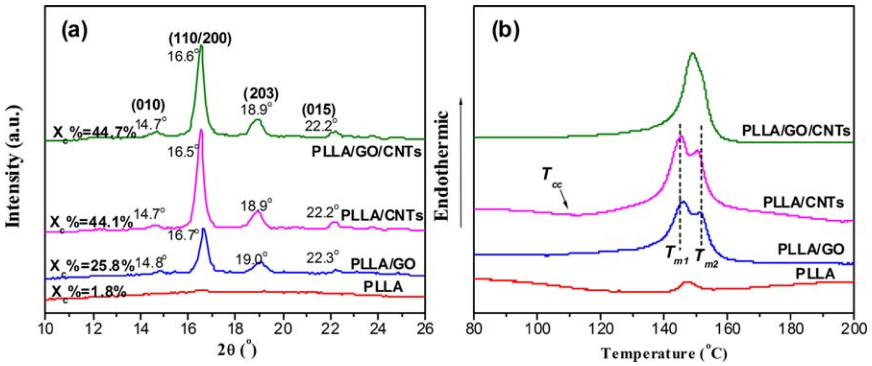

Figure 6. (a) WAXD profiles and (b) DSC heating curves of different samples which were prepared through isothermal crystallization process at 105°C for 30 min. The isothermal crystallization occurred from the melt. [Color figure can be viewed in the online issue, which is available at wileyonlinelibrary.com.]

the absolute value; however, the variation trend of X_{c-DSC} can reflect the variation of crystalline structure of the sample to a certain extent. Obviously, the simultaneous addition of GO and CNTs have more potential to enhance the crystallinity of PLLA matrix. As proved previously that GO exhibits percolated network structure while CNTs exhibit good dispersion in the PLLA matrix, therefore, it can be deduced that the reduced X_{c-DSC} of matrix in PLLA/GO sample is mainly attributed to the formation of network structure which possibly provides restriction for the growth of PLLA crystallites. The restriction can also be observed in the cold crystallization process, which results in a weak exothermic peak for PLLA/GO sample during the DSC heating process. For PLLA/GO/CNTs sample, although the percolated network structure is also detected, both GO and CNTs exhibit excellent dispersion in the PLLA matrix, and especially the presence of GO also facilitates the good dispersion of CNTs, which most likely results in more efficient nucleation effect of CNTs for PLLA crystallization during the nonisothermal crystallization process, leading to the great increase of X_{c-DSC} of PLLA matrix in PLLA/GO/CNTs sample.

Figure 6 shows the crystalline structure and melt behaviors of PLLA nanocomposites obtained through isothermal crystallization at 105°C for 30 min. It should be stressed that the crystallization occurred from the melt. As it is well known, the crystallization ability of PLLA is relatively small and it can not crystallize at the relatively higher cooling rate. Therefore, it can be pointed out that whether during the cooling scan from the melt to the temperature of 105°C or during the cooling scan from 105°C to room temperature in the atmosphere condition, the crystallization of PLLA does not occur due to the higher cooling rate. Therefore, the actual crystalline structure of PLLA formed during the isothermal crystallization process can be detected by WAXD. As shown in Figure 6(a), pure PLLA exhibits a very weak diffraction peak at $2\theta = 16.6°$, attributing to the diffraction of (110)/(200) crystal planes. For PLLA/GO sample, besides the largely intensified diffraction peak of (110)/(200) crystal planes, the other characteristic diffraction peaks at $2\theta = 14.8°$, 19.0°, and 22.3°, attributing to the diffractions of (010), (203), and (015) crystal planes, respectively, can be observed. This clearly proves that the crystallinity of PLLA matrix is enhanced in the PLLA/GO sample. Further intensified diffraction peaks of matrix are observed for PLLA/CNTs, indicating the further enhancement of crystallinity in the sample. The similar variation trend of WAXD profile is observed for PLLA/GO/CNTs sample. The crystallinity (X_{c-WAXD}) calculated from WAXD profile is also shown in the graph. The synergistic effects of GO and CNTs in enhancing the crystallinity of PLLA matrix can be clearly observed. The melting behaviors of different nanocomposites are shown in Figure 6(b). It can be clearly seen that only PLLA/CNTs sample exhibits cold crystallization phenomenon at T_{cc} of about 112.2°C. A weak endothermic peak is observed for pure PLLA, further proving that the crystallization of the sample during the isothermal crystallization process is greatly limited. Double endothermic peaks are observed at 145 to 146°C (T_{m1}) and 150 to 151°C (T_{m2}) for PLLA/CNTs and PLLA/GO samples, also indicating the melt-recrystallization-melt process of PLLA crystallites. Interestingly, only one endothermic peak at 148.9°C is observed for PLLA/GO/CNTs sample, indicating at least that the crystalline structure in the PLLA/GO/CNTs is more perfect than those in the PLLA/GO and PLLA/CNTs samples. Similarly, the crystallinity was calculated and the data of X_{c-DSC} for pure PLLA, PLLA/GO, PLLA/CNTs and PLLA/GO/CNTs are 1.7, 24.3, 31.7, and 34.7%, respectively. The variation of X_{c-DSC} further proves the synergistic effects of GO and CNTs in enhancing the crystallinity of PLLA matrix during the isothermal crystallization process.

The different effects of GO and CNTs on PLLA crystallization are further analyzed by studying the cold crystallization behaviors of nanocomposites during the annealing process. It should be noticed that before annealing treatment at 120°C, all the samples were quenched in the ice-water and the samples were in the amorphous state. After being annealed, the samples were cooled to room temperature and then analyzed by DSC. As shown in Figure 7(a), pure PLLA exhibits an intense diffraction peak at $2\theta = 16.4°$, also attributing to the diffraction of (110)/(200) crystal planes. However, it should be stressed that in the sample, the main crystalline structure is αÇ-form rather than the α-form[50] possibly due to that the crystallization occurs from the solid state and the chain segments have limited mobility, which leading to the formation of αÇ-form with imperfect crystalline structure. The X_{c-WAXD} of PLLA was calculated as 20.0%, further indicating the occurring of cold crystallization of pure PLLA during the

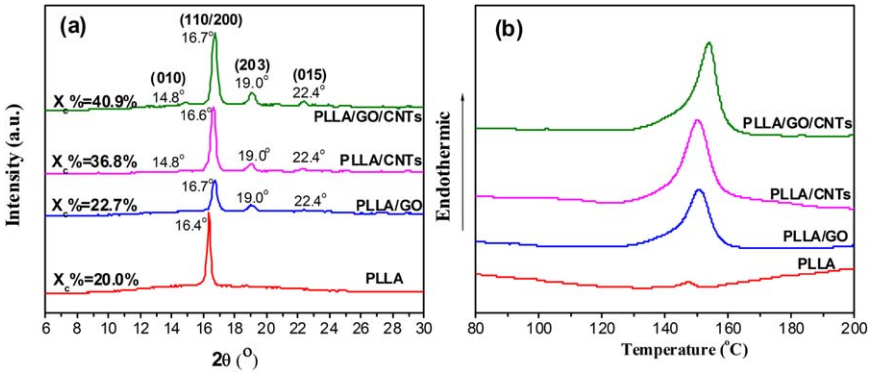

Figure 7. (a) WAXD profiles and (b) DSC heating curves of annealed samples which were prepared through annealing at 120°C for 30 min. The samples were quenched into the amorphous state and then annealed at 120°C. After that, the samples were cooled and analyzed by DSC. [Color figure can be viewed in the online issue, which is available at wileyonlinelibrary.com.]

annealing process. Almost all the annealed nanocomposites exhibit more complicated WAXD profiles compared with annealed pure PLLA. Specifically, one can see that the diffraction peaks of (110)/(200) crystal planes for all the nanocomposites are present at relatively higher 2θ values, indicating that the main crystalline structure in the nanocomposites is α-form. Similar to the observations obtained from the WAXD measurements of isothermally crystallized samples, annealed PLLA/GO sample exhibits the smallest X_{c-WAXD} among the three nanocomposites whereas PLLA/GO/CNTs exhibits the biggest one. This further indicates that the percolated network structure of GO is unfavorable for the crystallization of PLLA matrix on the one hand. On the other hand, GO and CNTs exhibit synergistic effects in improving the cold crystallization of PLLA matrix during the annealing process when they are present simultaneously in the nanocomposite. As shown in Figure 7(b), besides pure PLLA which exhibits a weak endothermic peak at T_m of 147.1°C, all the nanocomposites exhibit single endothermic peaks with increased T_m values compared with the isothermally crystallized samples, which indicates that the crystalline structures of annealed nanocomposites are relatively more perfect than those obtained from isothermal crystallization process possibly due to the relatively high annealing temperature facilitating the thickening of PLLA lamellae. The crystallinity was also calculated and the data of X_{c-DSC} for pure PLLA, PLLA/GO, PLLA/CNTs and PLLA/GO/CNTs are 1.1, 26.0, 29.9, and 36.3%, respectively. The observations of crystallinity of nanocomposites obtained from DSC measurement agree well with those obtained from previous WAXD measurement. The different is that for pure PLLA, WAXD profile shows the presence of a large amount of crystalline structure in the sample and the X_{c-WAXD} is about 20.0%, however, DSC measurement shows that the amount of crystalline structure in the same sample is very few and the X_{c-DSC} is only 1.1%. Both WAXD and DSC measurements were repeated for several times and the similar results are reported. This can be attributed to the phase transition between αÇ-form and α-form of PLLA during the heating process. It is known to all that αÇ-form is a metastable phase and has a tendency to change into more stable α-form through melt-recrystallization process companioned with the exothermic phenomenon.[46,50] As shown in Figure 7(b), one can notice that the DSC curve levels off at temperature higher than 100°C and maintains the state in a wide range from 100 to 140°C, indicating the continuous heat release process. Although the stable α-form further melts at relatively higher temperature and gives the endothermic peak, the intensity of the endothermic peak is counteracted by exothermic peak originated from αÇ→α transition. As a consequence, only a weak endothermic peak is observed for annealed pure PLLA. Further work should be done using temperature-modulated DSC (TMDSC) to understand the phase transition of PLLA during the heating process.

Thermal Stability of Nanocomposites

Generally, the presence of nanofiller facilitates the improvement of thermal stability of polymer matrix due to the increase of thermal conductivity and the shield effect of nanofiller. Nanofiller with sheet structure is believed to be the ideal modifier to improve the thermal stability of polymer matrix attributing to the barrier effect originated by the high aspect ratio sheets, which are dispersed homogeneously in the matrix delaying the escape of volatile degradation products within the nanocomposite.[52,53] Further researches show that if nanofillers with different dimensions are present simultaneously, polymer nanocomposites exhibited enhanced thermal stability compared with the binary nanocomposites with only one type of nanofiller, indicating the synergistic effects of nanofillers in improving thermal stability possibly due to the formation of a more efficient percolated network structure with significantly reduced mobility of polymer chains.[54,55]

As proved previously, when GO and CNTs are present in the PLLA matrix simultaneously, the rheological measurement proves the presence of percolated network structure in the matrix. Specifically, UV-Vis results show that the presence of GO facilitates the good dispersion of CNTs. Therefore, it is reasonable to be believed that the sample containing GO and CNTs simultaneously will exhibit excellent thermal stability. To prove this, the effect of nanofiller on thermal stability of PLLA matrix was investigated using TGA. Figure 8 shows the TGA curves of pure PLLA and nanocomposites obtained at different heating rates in nitrogen atmosphere. At relatively lower heating rate, i.e. 10°C/min [seen in Figure 8(a)], the temperatures corresponding to the weight loss of 5 wt % ($T_{5wt\%}$) and

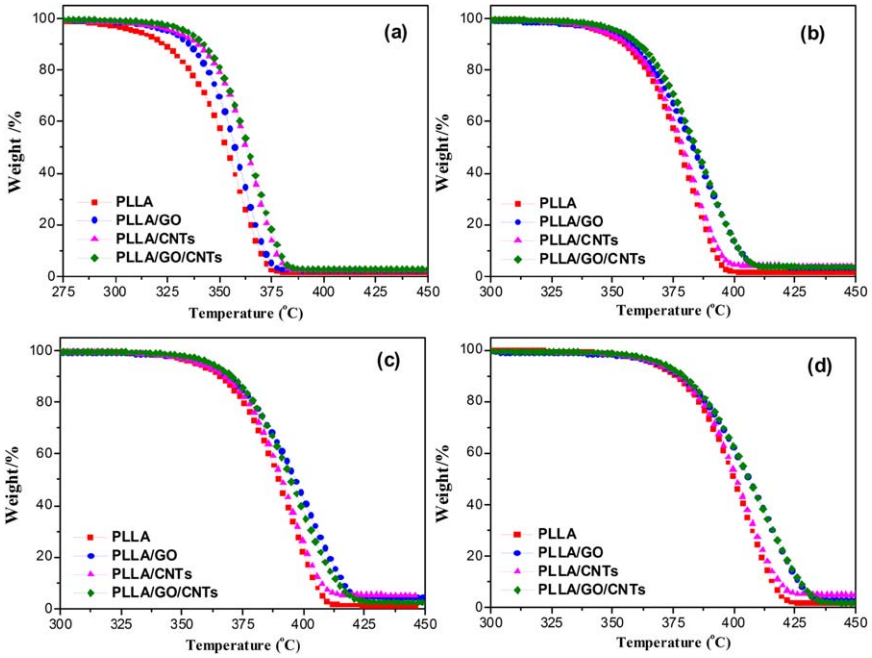

Figure 8. TGA curves of different samples obtained at different heating rates with nitrogen atmosphere. (a) 10°C/min, (b) 20°C/min, (c) 30°C/min, and (d) 40°C/min. [Color figure can be viewed in the online issue, which is available at wileyonlinelibrary.com.]

95 wt % ($T_{95wt}\%$) of pure PLLA are 310.3 and 372.4°C, respectively, and the temperature corresponding to the maximum rate of decomposition ($T_{d-\max}$) is 359.9°C. For PLLA/GO sample, the corresponding data are enhanced to 325.4, 360.7 and 375.2°C for $T_{5wt}\%$, $T_{d-\max}$, and $T_{95wt}\%$, respectively, indicating that GO exhibits apparent role in improving the thermal stability of PLLA matrix. Further enhanced thermal properties are observed for PLLA/CNTs and PLLA/GO/CNTs samples. For the former sample, the data of $T_{5wt}\%$, $T_{d-\max}$, and $T_{95wt}\%$ are 327.6, 366.9, and 380.1°C, respectively. For the latter one, the data are 333.8, 366.8, and 381.9°C, respectively. Obviously, there are synergistic effects of GO and CNTs in improving the thermal stability of PLLA matrix, especially at the initial stage of thermal decomposition of material. With the increase of heating rate [seen in Figure 8(b–d)], the TGA curves of all the samples shift to higher temperatures and the corresponding data increases accordingly. This can be attributed to the shorter time required for the sample to reach a given temperature. The variations of $T_{5wt}\%$ and $T_{d-\max}$ versus the heating rate are shown in Figure 9. It can be seen that in the initial stage of thermal decomposition, pure PLLA has the smallest $T_{5wt}\%$ while PLLA/GO/CNTs exhibits the biggest $T_{5wt}\%$, further indicating the synergistic effects of GO and CNTs in preventing the decomposition of PLLA matrix. However, it should be noticed that the synergistic effects are dependent upon the heating rate. The smaller the heating rate used in the TGA measurement, the more apparent are the synergistic effects of GO and CNTs in improving the thermal stability of PLLA. From Figure 9(b) one can see that the synergistic effects of GO and CNTs also become inconspicuous at the temperature which the maximum decomposition rate takes place [seen in Figure 9(b)].

The energy of activation during the thermal decomposition can be calculated from TGA curves according to the methodology developed by isoncoversional model-free kinetic analysis,[56] which has to perform a series of runs with different temperature program according to the literature.[57] It is also recommended

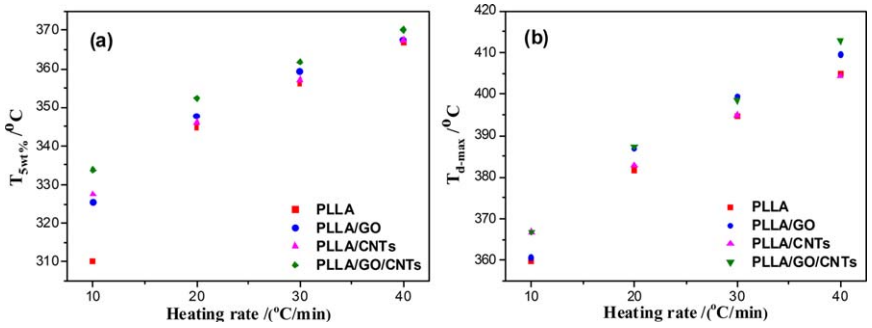

Figure 9. Comparison of thermal stability parameters of different samples obtained at different heating rates. (a) $T_{5wt}\%$ and (b) $T_{d-\max}$. [Color figure can be viewed in the online issue, which is available at wileyonlinelibrary.com.]

Table III. Activation Energy of Pure PLLA and PLLA Nanocomposites

Samples	E_a (kJ/mol)
PLLA	193.7
PLLA/GO	177.6
PLLA/CNTs	227.7
PLLA/GO/CNTs	201.3

The TGA measurement was carried out in nitrogen and the heating rate was 10°C/min.

to determine the E_a values in a wide range of $\alpha = 0.05–0.95$ with a step of not larger than 0.05. The formula is shown as follows:

$$\ln\left[\beta_i\left(\frac{d\alpha}{dT}\right)_{\alpha,i}\right]=\ln\left[A_\alpha f(\alpha)\right]-\frac{E_a}{RT_{\alpha,i}} \quad (3)$$

where the subscript α indicates the isoconversional values, i.e. the values related to a given extent of conversion. The subscript i denotes the various temperature programs. E_a is the activation energy, A_α is the pre-exponential factor, R is the universal gas constant and $f(\alpha)$ is the reaction model, β_i is the heating rates, and T is temperature. Therefore, a plot of $\ln\left[\beta_i\left(\frac{d\alpha}{dT}\right)_{\alpha,i}\right]$ versus $\frac{1}{T_{\alpha,i}}$ provides a straight line with the slop of $-\frac{E_a}{R}$. In this work, the α values ranged from 0.10 to 0.40 in order to ensure the fitting curve is a straight line. Consequently, E_a can be achieved through the value of slop and the results are shown in Table III. It can be seen that pure PLLA exhibits the E_a of 193.7 kJ/mol. With the presence of GO, the E_a is decreased to 177.6 kJ/mol. This might be ascribed to the catalyzed degradation induced by the functional groups on the GO surface. For PLLA/CNTs sample, the E_a increased to 227.7 kJ/mol. This means that CNTs can enhance the thermal degradation activation energy of the nanocomposites dramatically. The PLLA/GO/CNTs sample exhibits the E_a of 201.3 kJ/mol. Although the value is smaller than that of PLLA/CNTs sample, but it is still higher than that of PLLA/GO sample. Since the E_a is calculated during the process that the α values is bigger than 0.05, GO and CNTs do not show the synergistic effect in enhancing the E_a. Therefore, it can be concluded that GO and CNTs can exhibit the synergistic effect in improving the thermal stability of the PLLA; however, once the thermal decomposition occurs, the synergistic effect is disappeared.

CONCLUSIONS

In summary, three different PLLA nanocomposites containing GO, CNTs, and the compound of GO/CNTs were prepared, respectively. UV-Vis spectroscopy measurement show that the simultaneous presence of GO and CNTs is favorable for the good dispersion of the two nanofillers. The results obtained from SEM and rheological measurement show that all the nanofillers exhibit good dispersion in the PLLA matrix, and especially when GO and CNTs are present simultaneously, the dispersion of CNTs is further improved and the percolated network structure of GO and CNTs is detected. The study on the crystallization behavior of PLLA matrix under the different conditions shows that both GO and CNTs exhibit the role of nucleation agent to promote the crystallization of PLLA matrix. Due to the improved dispersion of nanofillers induced by the presence of GO and CNTs, the ternary nanocomposite exhibits improved crystallization ability and largely enhanced crystallinity compared with the binary nanocomposites containing only one type of nanofiller. The results obtained from TGA measurements show that both GO and CNTs have apparent roles in enhancing the thermal stability of PLLA matrix. Our results clearly indicate that there are synergistic effects of GO and CNTs in improving the crystallization and thermal stability of PLLA. This is very significant with respect to the preparation of new PLLA materials with enhanced crystallization ability and functional properties.

Authors express their sincere thanks to the National Natural Science Foundation of China (51203129, 50973090), Distinguished Young Scholars Foundation of Sichuan (2012JQ0057), and the Fundamental Research Funds for the Central Universities (SWJTU12CX010, SWJTU11CX142, SWJTU11ZT10) for financial support.

REFERENCES

1. Zhang, C.; Tjiu, W. W.; Liu, T. X.; Lui, W. Y.; Phang, I. Y. Zhang, W. D. *J. Phys. Chem. B* **2011**, *115*, 3392.
2. Palza, H.; Reznik, B.; Wilhelm, M.; Arias, O.; Vargas, A. *Macromol. Mater. Eng.* **2012**, *297*, 474.
3. Lu, M.; Lau, K. T.; Tam, W. Y.; Liao, K. *Carbon.* **2006**, *44*, 381.
4. Beryer, G. *Fire. Mater.* **2005**, *29*, 61.
5. Geng, C.; Wang, J.; Zhang, Q.; Fu, Q. *Polym. Int.* **2012**, *61*, 934.
6. Dubois, P.; Alexandre, M. *Adv. Eng. Mater.* **2006**, *8*, 147.
7. Peeterbroeck, S.; Lepoittevin, B.; Pollet, E;. Benali, S.; Broekaert, C.; Alexandre, M.;Bonduel, D.; Viville, P.; Lazzaroni, R.; Dubois, P. *Polym. Eng. Sci.* **2006**, *46*, 1022.
8. Zhang, W. D.; Phang, I. Y.; Shen, L.; Chow, S. Y.; Liu, T. X. *Macromol. Rapid. Commun.* **2004**, *25*, 1860.
9. Costache, M.C.; Wang, D.; Heidecker, M. J. Mnias, E.; Wilkier, C.A. *Polym. Adv. Technol.* **2006**, *17*, 272.
10. Ma, H. Y.; Tong, L. F.; Xu, Z. B.; Fan, Z. P. *Nanotechnology* **2007**, *18*, 375602.
11. Tang, C. Y.; Xiang, L.X.; Su, J. X.; Wang, K.; Yang, C. Y.; Zhang, Q.; Fu, Q. *J. Phys. Chem. B* **2008**, *112*, 3876.
12. Liu, L.; Grunlan, J. C. *Adv. Funct. Mater.* **2007**, *17*, 2343–2348.
13. Yang, S. Y.; Lin, W. N.; Huang, Y. L.; Tien, H. W.; Wang, J. Y.; Ma, C. C.M.; Li, S. M.; Wang, Y. S. *Carbon* **2011**. *49*. 793.
14. Hu, H. Q.; Zhao,L.; Liu, J. Q.; Liu, Y.; Cheng, J. M.; Luo, J.; Liang Y. R.; Tao, Y.; Wang, X.; Zhao, J. *Polymer* **2012**. *53*. 3378.
15. Tian, L. L.; Meziani, M. M.; Lu, F.; Kong, C. Y.; Cao, L.; Thorne, T. J.; Sun, Y. P. *Appl. Mater. Int.* **2010**, *2*, 3217.
16. Zhang, C.; Ren, L. L.; Wang, X. Y.; Liu, T. X. *J. Phys. Chem. C* **2010**, *114*, 11435–11440.
17. Zhang, C.; Huang, S.; Tjiu, W. W.; Fan, W.; Liu, T. X. *J. Mater. Chem.* **2012**, *22*, 2427–2434.

18. Wu, D. F.; Wu, L.; Zhou, W. D.; Zhang, M.; Yang, T. *Polym. Eng. Sci.* **2010**, *50*, 1721.
19. Zhao, Y. Y.; Qiu, Z. B.; Yan, S. K.; Yang, W. T. *Polym. Eng. Sci.* **2011**, *51*, 1564.
20. Barrau, S.; Vanmmansart, C.; Moreau, M.; Addad, A.; Stoclet, G.; Lefebvre, J. M.; Seguela, R. *Macromolecules* **2011**, *44*, 6496.
21. Shieh, Y. T.; Twu, Y. K.; Su, C. C.; Lin, R. H.; Liu, G. L. *J. Polym. Sci. Part B: Polym. Phys.* **2010**. *48*, 983.
22. Yoon, J. T.; Lee, S. C.; Jeong, Y. G. *Compos. Sci. Technol.* **2010**, *70*, 776.
23. Xu Z. H.; Niu, Y. H.; Yang, L.; Xie, W. Y.; Li, H.; Gan, Z. H.; Wang, Z. G. *Polymer* **2010**, *51*, 730.
24. Chrissafis, K.; Paraskevopoulos, K. M.; Jannakoudakis, A.; Beslikas, T.; Bikiaris D. *J. Appl. Polym. Sci.* **2010**, *118*, 2712.
25. Wu, D. F.; Wu, L.; Zhou, W. D.; Sun, Y. R.; Zhang, M. *J. Polym. Sci. Part B: Polym. Phys.* **2010**, *48*, 479.
26. Xu, Z. H.; Niu, Y. H.; Wang, Z. G.; Li, H.; Yang, L.; Qiu, J.; Wang, H. *ACS Appl. Mater. Interfaces* **2011**, *3*, 3744.
27. Zhao, Y. Y.; Qiu, Z. B.; Yang, W. T. *Compos. Sci. Technol.* **2009**, *69*, 627.
28. Wu, D. F.; Wu, L.; Zhang, M.; Zhao, Y. L. *Polym. Degrad. Stab.* **2008**, *93*,1577.
29. Kim, H. S.; Chae, Y. S.; Kwon, H.; Yoon, J. S. *Polym. Int.* **2009**, *58*, 826.
30. Wang, H. S.; Qiu, Z. B. *Thermochim. Acta* **2011**, *526*, 229.
31. Sun, Y.; He, C. B. *ACS Macro Lett.* **2012**, *1*, 709.
32. Xu, J. Z.; Chen, T.; Yang, C. L.; Li, Z. M.; Mao, Y.M.; Zeng, B. Q.; Hsiao, B. S. *Macromolecules* **2010**, *43*, 5000.
33. Kim, H. S.; Kwon, H. I.; Kwon, S. M.; Yun, Y. S.; Yoon, J. S.; Jin, H. J. *J. Nanosci. Nanotechnol.* **2010**, *10*, 1533.
34. Hapuarachchi, T. D.; Peijs, T. *Compos. A* **2010**, *41*, 954.
35. Santangelo, S.; Gorrasi, G.; Lieto, R. D.; Pasquale, S. D.; Patimo, G.; Piperopoulos, E.; Lanza, M.; Faggio, G.; Mauriello, F.; Messina, G.; Milone, C. *Appl. Clay. Sci.* **2011**, *53*, 188.
36. Kovtyukhova, N. I.; Ollivier, P. J.; Martin, B. R.; Mallouk, T. R.; Chizhik, S. A.; Buzaneva, E. V.; Gorchinskiy, A. D. *Chem. Mater.* **1999**, *11*, 771.
37. Yang, J. H.; Feng, C. X.; Dai, J.; Zhang, N.; Huang, T.; Wang, Y. *Polym. Int.* **2013**, *62*, 1085.
38. Gao, Y.; Wang, Y.; Shi, J.; Bai, H. W.; Song, B. *Polym. Test.* **2008**, *27*, 179.
39. Javad, S.; Iman, H.; Gity Mir, M. S.; Seyed Mohammad, D.; Sadegh, G. *J. Appl. Polym. Sci.* **2012**, *123*, 2492.
40. Han, C. D.; Lem, K. W. *Polym. Eng. Rev.* **1983**, *2*, 135.
41. Pötschke, P.; Fornes, T. D.; Paul, D. R. *Polymer* **2002**, *43*, 3247.
42. McClory, C.; McNally, T.; Baxendale, M.; Pötschke, P.; Blau, W.; Ruether, M. *Eur. Polym. J.* **2010**, *46*, 854.
43. Khare, R. A.; Bhattacharyya, A. R.; Kulkarni, A. R.; Saroop, M.; Biswas, A. *J. Polym. Sci. Part B: Polym. Phys.* **2008**, *46*, 2286.
44. Cheng, H. K. F.; Sahoo, N. G.; Pan, Y. Z.; Chan, S. H.; Zhao, J. H.; Chen, G. *J. Polym. Sci. Part B: Polym. Phys.* **2010**, *48*, 1203.
45. Wu, D. F.; Zhang, Y.; Zhang, M.; Yu, W. *Biomacromolecules* **2009**, *10*, 417.
46. Zhang, J. M.; Tashiro, K.; Tsuji, H.; Domb, A. *J. Macromolecules* **2008**, *41*, 1352.
47. Zhang, J. M.; Duan, Y. X.; Sato, H.; Tsuji, H.; Noda, I.; Yan, S.; Ozaki, Y. *Macromolecules* **2005**, *38*, 8012.
48. Cho, T. Y.; Strobl, G. *Polymer* **2006**, *47*, 1036.
49. Pan PJ, Kai WH, Zhu B, Dong T, Inoue Y. *Macromolecules* **2007**, *40*, 6898.
50. Pan, P. J.; Zhu, B.; Kai, W. H.; Dong, T.; Inoue, Y. *Macromolecules* **2008**, *41*, 4296.
51. Villmow, T.; Pötschke, P.; Pegel, S.; Häussler, L.; Kretzschmar, B. *Polymer* **2008**, *49*, 3500.
52. Zanetti, M.; Camino, G.; Reichert, P.; Mulhaupt, R. *Macromol. Rapid Commun.* **2001**, *22*, 176.
53. Marras, S. I.; Zuburtikudis, I.; Panayiotou, C. *Eur. Polym. J.* **2007**, *43*, 2191.
54. Ma, H. Y.; Tong, L. F.; Xu, Z. B.; Fang, Z. P. *Nanotechnology* **2007**, *18*, 375602.
55. Palza, H.; Reznik, B.; Wilhelm, M.; Arias, O.; Vargas, A. *Macromol. Mater. Eng.* **2012**, *297*, 474.
56. Vyazovkin, S.; Sbirrazzuoli, N. *Macromol. Rapid Commun.* **2006**, *27*, 1515.
57. Vyazovkin, S.; Burnham, A. K.; Criado, J. M.; Perez-Maqueda, L. A.; Popescu, C.; Sbirrazzuoli, N. *Thermochim. Acta* **2011**, *520*, 1.